Acoustic Noise Reduction for Low-Speed Sensorless Operation of Dual Three-Phase PMSM With Random Winding Injection

Qiu, Xianqun; He, Yang; Zhao, Wenxiang; Sun, Mingyang; Zhou, Dao; Jin, Shibo

Published in:
I E E E Transactions on Energy Conversion

DOI (link to publication from Publisher):
10.1109/TEC.2023.3282609

Publication date:
2023

Document Version
Accepted author manuscript, peer reviewed version

Acoustic Noise Reduction for Low Speed Sensorless Drive of Dual Three-Phase PMSM

Xianqun Qiu, Wenxiang Zhao, *Senior Member, IEEE*, Mingyang Sun, Dao Zhou, *Senior Member, IEEE*, and Jinghua Ji

***Abstract*—This paper proposes a pseudorandom sinusoidal voltage signal with random winding injection method for acoustic noise reduction. Two fixed frequency signals are randomly selected as injection signals. Then, one of the two sets of windings of the dual three-phase permanent magnet synchronous motor (DTP-PMSM) is randomly chosen for injection. Due to this unique injection scheme, the injected frequency component in the response current can be reduced. Two pseudorandom numbers are generated synchronously by the digital signal system. The first random number selects two voltage signals with different frequencies. Meanwhile, one of the two sets of windings is chosen by the second random number. Thus, there is only one winding with the injection signal at a certain time. In order to obtain the position and speed of the motor, a corresponding high-frequency signal processing is presented. The power spectral density of the response current caused by the injected signal is also analyzed in this paper. Finally, the experimental results verify the proposed method.**

***Index Terms*—Acoustic noises reduction, dual three-phase motor, sinusoidal voltage injection, permanent-magnet synchronous motor (PMSM), sensorless control.**

I. Introduction

MULTI-PHASE motor drives have attracted significant attention due to the merits of high power, low dc-link voltage requirement, high reliability, and excellent fault-tolerant capability [1]. The dual three-phase permanent-magnet synchronous motor (DTP-PMSM) was discussed in some literature [2]-[5], which has two stator windings sets spatially shifted by $\pi/6$ with isolated neutral points. The DTP-PMSM has the intrinsic feature of elimination of sixth harmonic torque pulsation, high windings factor, and low stator magnetic motive force harmonic components [6]. As shown in Fig. 1, the two sets of relatively independent windings bring more flexibility to the control of the DTP-PMSM.

Sensorless control improves the reliability of the motor drive system by eliminating the mechanical sensor and its signal processing circuit. Meanwhile, the cost and size of the motor drive system can be reduced. According to the operating speed range of the motor, the position sensorless technology falls into two main categories: one relies on the back electromotive force voltage associated with the fundamental excitation of a machine (model-based methods for medium-high speed) [7]-[9], and other utilizes a second excitation signal superimposed on the fundamental excitation (saliency-based methods for standstill and low speed) [10]-[12].

The high-frequency signal injection method can be used to accurately estimate the rotor position at low speed without additional hardware [13]. According to the type of injected carrier signal, the high-frequency signal injection method includes sinusoidal injection, square-wave injection, triangular-wave injection, and arbitrary injection. Although the high-frequency signal injection method shows good performance at low speed, the adverse side effects of acoustic noise arising from high-frequency voltage injection are an issue that needs to be concerned.

Many efforts have been made to suppress undesirable acoustic noise [14]. Decreasing the injection signal amplitude is an intuitive solution to deal with the acoustic noise. However, the signal-to-noise ratio of the response signal drops inevitably. Thus, the position information obtained from the response signal is easily affected. The noise reduction can be achieved by adjusting the injection frequency out of the hearing range of the human ear. In order to improve dynamic performance and reduce the acoustic noise, the injection frequency and the switching frequency of pulse width modulation is increased in [15]. However, the switching loss caused by high-frequency injection cannot be ignored, and it is still challenging to exceed the hearing range of human ears. Since the low-frequency noise is softer than the high-frequency noise, lowering the injection frequency is another feasible way to reduce the acoustic noise [16], [24]. A low-frequency voltage injection is proposed in [16] by separating the injection and the control periods. An enhanced vector-tracking observer was designed to improve the accuracy of position estimation. However, the dynamic performance of position estimation is relatively poor, especially in load step conditions.

The pseudorandom high-frequency signal injection is another effective method to reduce acoustic noise, which has been verified in some literature. The pseudorandom-frequency signal injection scheme can convert the narrowband acoustic

This work was supported in part by the National Natural Science Foundation of China under Grant 52025073, and in part by the Graduate Scientific Research Innovation Project of Jiangsu Province under Grant KYCX20_2855, and in part by the Jiangsu Government Scholarship for Overseas Studies under Grant JS-2020-209, and in part by the Priority Academic Program Development of Jiangsu Higher Education Institutions. (*Corresponding author: Wenxiang Zhao*)

X. Qiu, W. Zhao, M. Sun and J. Ji are with the School of Electrical and Information Engineering, Jiangsu University, Zhenjiang 212013, China (e-mail: xianqunqiu@163.com; zwx@ujs.edu.cn; smy2434@163.com, jjh@ujs.edu.cn)

D. Zhou is with the AAU Energy, Aalborg University, 9220 Aalborg, Denmark (e-mail: zda@energy.aau.dk).

noises into broadband noises by spreading the high-frequency response current spectrum. A pseudorandom high-frequency voltage injection method for the random variations of square-wave voltages with two different frequencies is proposed in [17]. In [18], a hybrid pseudorandom signal injection was implemented by injecting signals with the frequency switching between two values, augmented with the phase toggling among four values in a random manner. The pseudorandom sinusoidal voltage injection also received attention for reducing acoustic noise, as presented in [19]. The system delays problem can be solved by an enhanced signal processing method without the participation of the demodulation signal. Meanwhile, the high-frequency current injection method was developed for reduces acoustic noise in [20] and [21]. In order to achieve better randomization performance, the Markov Chain model is discussed in [22] and [23]. Different from the innovation of generating random signals, [24] proposed a high-frequency signal injection scheme with a random switching frequency. The frequency of the injected high-frequency voltage and switching frequency are adjusted randomly. For the DTP-PMSM, the high-frequency injection method is an effective scheme for low-speed sensorless control. However, the DTP-PMSM sensorless control scheme also suffers from the acoustic noise caused by the injected signal. Besides, the power spectrum peak at the fixed frequency will be affected due to the mutual inductance of the two sets of windings. Although the pseudorandom frequency signal injection method mentioned above can have a certain effect on noise reduction, it cannot make further use of the characteristics of the DTP-PMSM.

In this paper, a pseudorandom sinusoidal signal with random winding injection method for the DTP-PMSM sensorless drive is proposed. The pseudorandom sinusoidal voltage signal is generated, which is randomly injected into the two sets of windings of the DTP-PMSM. Thus, the acoustic noise caused by the injected signal can be reduced. Correspondingly, the high-frequency signal processing for two sets of winding is devised to estimate the rotor position and speed. The rest of this paper is organized as follows. Section II briefly describes the sinusoidal voltage injection method. The proposed noise reduction sensorless control for the DTP-PMSM is presented in Section III. The analysis of power spectral density (PSD) is presented in Section IV. Section V provides experimental results to evaluate the performance of the proposed method. Finally, the conclusions are presented in Section VI.

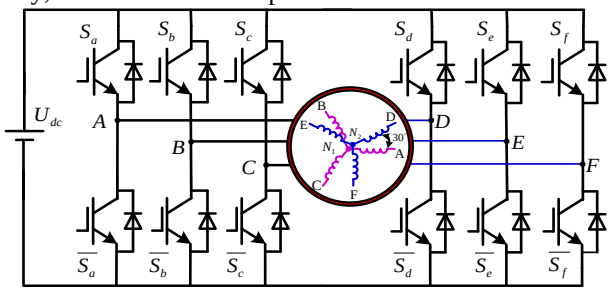

Fig. 1. DTP-PMSM drive system.

II. Sinusoidal Signal Injection Method

The two stator windings sets of DTP-PMSM can be assumed as symmetrical, only different in spatial distribution. Thus, the position estimation model for two sets of windings is the same. The winding ABC and winding DEF is defined as winding 1 and winding 2. θ_{e1} and θ_{e2} are the real position for winding 1 and winding 2, respectively. The winding 1 and winding 2 have the same parameters of inductance and resistance, i.e. $L_{d1} = L_{d2} = L_d$, $L_{q1} = L_{q2} = L_q$, and $R_1 = R_2 = R$. The coordinate systems of DTP-PMSM can be built as shown in Fig. 2. The superscript "^" in this paper denotes the estimated axis or components.

When a dual DQ control scheme is applied, the high-frequency model of winding 1 can be expressed as

$$\begin{bmatrix} u_{d1h} \\ u_{q1h} \end{bmatrix} = \begin{bmatrix} sL_{dh} & 0 \\ 0 & sL_{qh} \end{bmatrix} \begin{bmatrix} i_{d1h} \\ i_{q1h} \end{bmatrix} \tag{1}$$

where s is the derivative operator, L_{dh} and L_{qh} are the high-frequency inductances of dq-axis, u_{d1h}, $u_{q1h,}$ and i_{d1h}, i_{q1h} are the high-frequency voltages and currents in the rotor frame of winding 1, respectively. The high-frequency voltage is injected into d_1-axis, which can be expressed as

$$\begin{bmatrix} \hat{u}_{d1h} \\ \hat{u}_{q1h} \end{bmatrix} = \begin{bmatrix} u_{inj} \\ 0 \end{bmatrix} = \begin{bmatrix} V_h \sin(\omega_h t) \\ 0 \end{bmatrix} \tag{2}$$

The transformation matrix $T(\Delta\theta_{e1})$ from the actual dq-axis to the estimated dq-axis can be expressed as

$$T(\Delta\theta_{e1}) = \begin{bmatrix} \cos(\Delta\theta_{e1}) & -\sin(\Delta\theta_{e1}) \\ \sin(\Delta\theta_{e1}) & \cos(\Delta\theta_{e1}) \end{bmatrix} \tag{3}$$

with

$$\Delta\theta_{e1} = \theta_{e1} - \hat{\theta}_{e1} \tag{4}$$

By combining (1), (2), and (3), the high-frequency current in the rotor frame can be expressed as

$$\begin{bmatrix} i_{d1h} \\ i_{d2h} \end{bmatrix} = \begin{bmatrix} sL_{dh} & 0 \\ 0 & sL_{qh} \end{bmatrix}^{-1} T^{-1}(\Delta\theta_{e1}) \begin{bmatrix} \hat{u}_{d1h} \\ \hat{u}_{d2h} \end{bmatrix} \tag{5}$$

meanwhile, the high-frequency current in the stator frame can be achieved as

$$\begin{bmatrix} i_{\alpha1h} \\ i_{\beta1h} \end{bmatrix} = \frac{u_{inj}}{sL_{dh}L_{qh}} \begin{bmatrix} L_{qh}\cos\theta_{e1}\cos\Delta\theta_{e1} + L_{dh}\sin\theta_{e1}\sin\Delta\theta_{e1} \\ L_{qh}\sin\theta_{e1}\cos\Delta\theta_{e1} - L_{dh}\cos\theta_{e1}\sin\Delta\theta_{e1} \end{bmatrix} \tag{6}$$

When $\Delta\theta_{e1}$ is small enough, (6) can be equivalent to

$$\begin{bmatrix} i_{\alpha1h} \\ i_{\beta1h} \end{bmatrix} = \frac{u_{inj}}{sL_{dh}} \begin{bmatrix} \cos\theta_{e1} \\ \sin\theta_{e1} \end{bmatrix} = \frac{-V_h\cos(\omega_h t)}{\omega_h L_{dh}} \begin{bmatrix} \cos\theta_{e1} \\ \sin\theta_{e1} \end{bmatrix} \tag{7}$$

then, with the aid of demodulation signal $-\cos(\omega_h t)$ and a low-pass filter, (7) can be rewritten as

$$\begin{bmatrix} i^*_{\alpha1h} \\ i^*_{\beta1h} \end{bmatrix} = LPF\left[-\cos(\omega_h t) \bullet \begin{bmatrix} i_{\alpha1h} \\ i_{\beta1h} \end{bmatrix} \right] = \frac{V_h}{\omega_h L_{dh}} \begin{bmatrix} \cos\theta_{e1} \\ \sin\theta_{e1} \end{bmatrix} \tag{8}$$

According to (8), the estimated position for winding 1 can be achieved by utilizing a phase-locked loop observer. Similarly, the sinusoidal signal injection method can be applied to winding 2. Therefore, the two sets of winding of the DTP-PMSM can be controlled separately. It should be noted that a harsh acoustic noise is inevitable due to the fixed high-frequency response current. Meanwhile, two sets of

demodulation programs also add a computational burden to the control system.

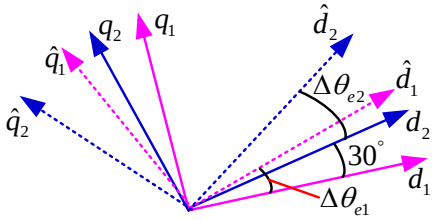

Fig. 2. Rotor coordinate systems for two sets of windings.

III. Proposed Pseudorandom Signal Injection Method

A. Pseudorandom Sinusoidal Injection

Compared with the fixed frequency sinusoidal injection method, the pseudorandom frequency sinusoidal injection can reduce the acoustic noise by spreading the high-frequency response current spectrum. In general, two sinusoidal signals with different frequencies are chosen in the conventional pseudorandom frequency sinusoidal injection method.

Fig. 3 shows the proposed pseudorandom voltage signal module for the DTP-PMSM. This process mainly includes two steps. The first step is to choose the injection signal. The higher and lower frequency injection signals can be defined as u_{inj1} and u_{inj2}. V_1, V_2, ω_1, and ω_2 are the amplitudes and angular frequencies of the injection signals, respectively. To keep the identical signal-to-noise ratio, the ratio of the amplitude and frequency of the injected signal is equal, i.e., $V_1 / \omega_1 = V_2 / \omega_2$. The digital signal system generates a pseudorandom number P between 0 and 1, which can be used to select the injection signal. If P is less than the switching probability K, i.e., P < K, the higher frequency signal u_{inj1} is injected into the system. Otherwise, the signal u_{inj2} is injected. Then, the second step is to choose the injected winding. Another pseudorandom number Q is generated to decide the injected winding. When Q is larger than K, the injection signal will be superimposed in winding 2. Otherwise, winding 1 is chosen as the injected winding. It is worth noting that the probabilities of the higher frequency signal and the winding chosen are both 50%. After a complete cycle of the injection signal, the pseudorandom numbers P and Q will be updated separately, and the procedures are repeated as mentioned above.

The pseudorandom sinusoidal signal waveform on winding 1 and winding 2 are shown in Fig. 4. U_{dh} represents the complete pseudorandom signal waveform. U_{d1h} and U_{d2h} represent the pseudorandom signal waveform for winding 1 and winding 2, respectively. It can be seen that the two injected signals on winding 1 and winding 2 are complementary. Thus, the high-frequency component in the winding can be reduced when the amplitude of the injected signal remains unchanged.

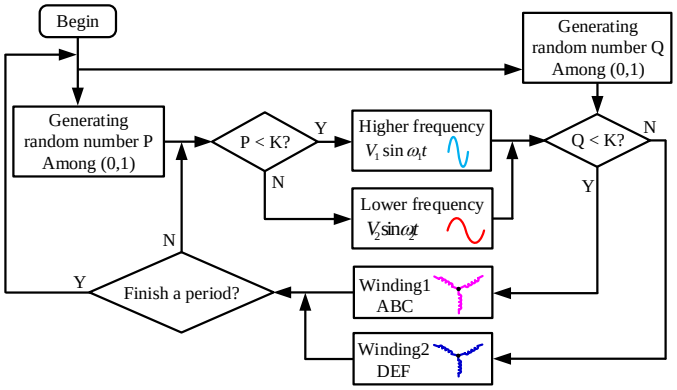

Fig. 3. Random voltage signal module for DTP-PMSM.

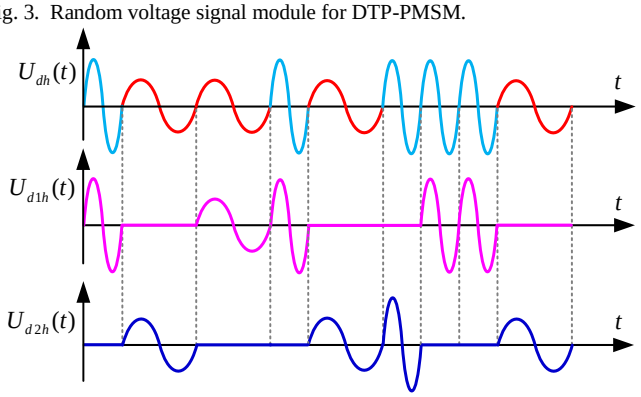

Fig. 4. Random sinusoidal voltage waveform.

B. High-Frequency Signal Processing

The high-frequency response current in $\alpha\beta_1$-axis and $\alpha\beta_2$ -axis can be obtained by the high-pass filter. In order to synthesize a complete high-frequency response current signal, the injected signal of winding 2 should be adjusted to π/6 ahead. The phase shift adjustment for winding 2 can be realized with the transformation, which can be described as

$$\begin{bmatrix} i^*_{\alpha 2h} \\ i^*_{\beta 2h} \end{bmatrix} = T^{-1}(\theta_{e2} + \frac{\pi}{6}) \begin{bmatrix} i_{d2h} \\ i_{q2h} \end{bmatrix} \tag{9}$$

When the adjustment is complete, a new coordinate system can be synthesized by winding 1 and winding 2, as shown in Fig. 5. The stator frame $\alpha\beta$-axis is synthesized by $\alpha\beta_1$-axis and $\alpha\beta_2$-axis, and the rotor frame dq-axis is synthesized by dq_1-axis and dq_2-axis. θ_e denotes the postion of dq-axis, and $\theta_e = \theta_{e1} = \theta_{e2} + \pi/6$. Meanwhile, the high-frequency current of $\alpha\beta$-axis can be given as

$$\begin{cases} i_{\alpha h} = i_{\alpha 1h} + i^*_{\alpha 2h} \\ i_{\beta h} = i_{\beta 1h} + i^*_{\beta 2h} \end{cases} \tag{10}$$

According to (6), (9) can be expressed as

$$\begin{bmatrix} i^*_{\alpha 2h} \\ i^*_{\beta 2h} \end{bmatrix} = \frac{u_{inj}}{sL_{dh}L_{qh}} \begin{bmatrix} L_{qh}\cos(\theta_e)\cos\Delta\theta_{e2} + L_{dh}\sin(\theta_e)\sin\Delta\theta_{e2} \\ L_{qh}\sin(\theta_e)\cos\Delta\theta_{e2} - L_{dh}\cos(\theta_e)\sin\Delta\theta_{e2} \end{bmatrix} \tag{11}$$

By utilizing (6), (10), and (11), the high-frequency current in the $\alpha\beta$-axis can be rewritten as

$$\begin{bmatrix} i_{\alpha h} \\ i_{\beta h} \end{bmatrix} = \frac{u_{inj}}{s} \begin{bmatrix} \dfrac{\cos\theta_e(\cos\Delta\theta_{e1} + \cos\Delta\theta_{e2})}{L_{dh}} + \dfrac{\sin\theta_e(\sin\Delta\theta_{e1} + \sin\Delta\theta_{e2})}{L_{qh}} \\ \dfrac{\sin\theta_e(\cos\Delta\theta_{e1} + \cos\Delta\theta_{e2})}{L_{dh}} - \dfrac{\cos\theta_e(\sin\Delta\theta_{e1} + \sin\Delta\theta_{e2})}{L_{qh}} \end{bmatrix} \tag{12}$$

when $\Delta\theta_{e1} \approx 0$, and $\Delta\theta_{e2} \approx 0$, (12) is approximated as

$$\begin{bmatrix} i_{\alpha h} \\ i_{\beta h} \end{bmatrix} = \frac{u_{inj}}{sL_{dh}} \begin{bmatrix} \cos\theta_e \\ \sin\theta_e \end{bmatrix} \tag{13}$$

In order to extract the position information from the high-frequency current in the $\alpha\beta$-axis, a rotor coordinate system for signal processing is built, as shown in Fig. 6. The coordinate frame is defined as dq^v-axis, which lags π/4 behind the synthetic estimated axis. Then, the high-frequency response current in the dq^v-axis can be expressed as

$$\begin{bmatrix} i_{dh}^v \\ i_{qh}^v \end{bmatrix} = T^{-1}(\hat{\theta}_e - \frac{\pi}{4}) \begin{bmatrix} i_{\alpha h} \\ i_{\beta h} \end{bmatrix}$$

$$= \frac{\sqrt{2}}{2} \frac{u_{inj}}{s} \begin{bmatrix} \frac{\cos^2\Delta\theta_e}{L_{dh}} - \frac{\sin^2\Delta\theta_e}{L_{qh}} + \frac{L_{dif}}{L_{dh}L_{qh}} \sin(2\Delta\theta_e) \\ \frac{\cos^2\Delta\theta_e}{L_{dh}} - \frac{\sin^2\Delta\theta_e}{L_{qh}} - \frac{L_{dif}}{L_{dh}L_{qh}} \sin(2\Delta\theta_e) \end{bmatrix} \tag{14}$$

where $\Delta\theta_e$ is the position estimation error between the actual and estimated position for the coordinate system, $L_{dif} = (L_{dh} - L_{qh}) / 2$. When $\Delta\theta_e \approx 0$, (14) can be rewritten as

$$\begin{bmatrix} i_{dh}^v \\ i_{qh}^v \end{bmatrix} = \frac{\sqrt{2}}{2} \frac{u_{inj}}{sL_{dh}L_{qh}} \begin{bmatrix} L_{qh} + L_{dif} \sin(2\Delta\theta_e) \\ L_{qh} - L_{dif} \sin(2\Delta\theta_e) \end{bmatrix} \tag{15}$$

Obviously, $L_{qh} > L_{dif}$. The part of (15) can be determined as

$$(L_{qh} \pm L_{dif} \sin(2\Delta\theta_e)) > 0 \tag{16}$$

In order to obtain the positive coefficient, the absolute value of high-frequency current can be achieved as

$$\begin{bmatrix} |i_{dh}^v| \\ |i_{qh}^v| \end{bmatrix} = \frac{\sqrt{2}}{2} \frac{u_{inj}}{sL_{dh}L_{qh}} \begin{bmatrix} L_{qh} + L_{dif} \sin(2\Delta\theta_e) \\ L_{qh} - L_{dif} \sin(2\Delta\theta_e) \end{bmatrix} \tag{17}$$

By utilizing the transformation, the high-frequency current in the $\alpha\beta^v$-axis can be calculated as

$$\begin{bmatrix} i_{\alpha h}^v \\ i_{\beta h}^v \end{bmatrix} = T(\hat{\theta}_e - \frac{\pi}{4}) \begin{bmatrix} i_{dh}^v \\ i_{qh}^v \end{bmatrix} = \frac{u_{inj}}{s} \begin{bmatrix} \frac{\cos\theta_e \cos\Delta\theta_e}{L_{dh}} + X_1 \\ \frac{\sin\theta_e \cos\Delta\theta_e}{L_{dh}} + X_2 \end{bmatrix} \tag{18}$$

with

$$\begin{cases} X_1 = L_{qh} \sin\theta_e \sin\Delta\theta_e + L_{dif} \sin\hat{\theta}_e \sin(2\Delta\theta_e) \\ X_2 = -L_{qh} \cos\theta_e \sin\Delta\theta_e - L_{dif} \cos\hat{\theta}_e \sin(2\Delta\theta_e) \end{cases} \tag{19}$$

when $\Delta\theta_e \approx 0$, $X_1 = X_2 \approx 0$. (18) can be simplified as

$$\begin{bmatrix} i_{\alpha h}^v \\ i_{\beta h}^v \end{bmatrix} = \frac{u_{inj}}{sL_{dh}} \begin{bmatrix} \cos\theta_e \\ \sin\theta_e \end{bmatrix} \tag{20}$$

When the motor operates at low speed, the electrical frequency is much smaller than the frequency of the injected signal. In order to ensure the integrator value of the injected signal is positive, the high-frequency currents in (20) should be processed by the low-pass filter. Moreover, the complexity of the parameters design can be reduced by using the normalization method. Thus, the final result after normalization can be expressed as

$$\begin{bmatrix} i_{\alpha o}^v \\ i_{\beta o}^v \end{bmatrix} = \frac{1}{\sqrt{LPF(i_{\alpha h}^v)^2 + LPF(i_{\beta h}^v)^2}} \begin{bmatrix} LPF(i_{\alpha h}^v) \\ LPF(i_{\beta h}^v) \end{bmatrix} = \begin{bmatrix} \cos\theta_e \\ \sin\theta_e \end{bmatrix} \tag{21}$$

According to (21), the position error ε can be obtained as

$$\varepsilon = i_{\beta o}^v \cos(\hat{\theta}_e) - i_{\alpha o}^v \sin(\hat{\theta}_e) = \sin(\Delta\theta_e) \approx \Delta\theta_e \tag{22}$$

The position error can be controlled by utilizing a phase-locked loop observer. The rotor speed and position can be obtained, as well as the position for winding 1 and winding 2. The block diagram of high-frequency signal processing is shown in Fig. 7.

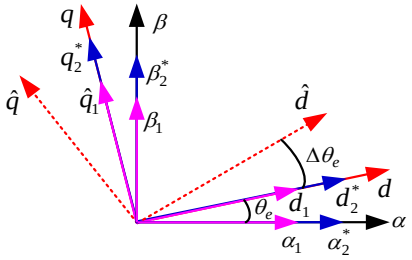

Fig. 5. Synthesize coordinate systems.

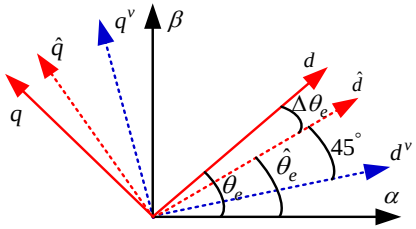

Fig. 6. Rotor coordinate system for signal processing.

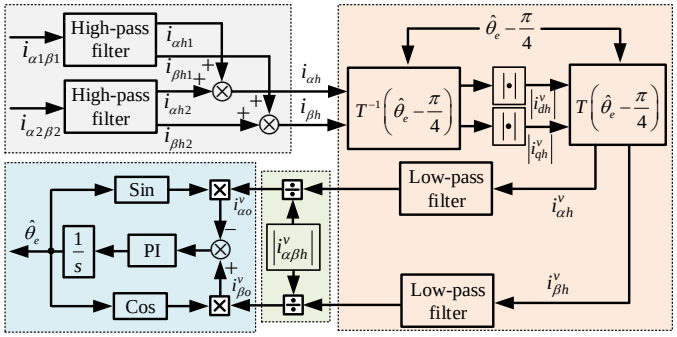

Fig. 7. Signal processing based on the proposed method.

IV. Analysis of PSD

Since a random signal is an infinite energy signal, its Fourier transformation does not exist. In order to analyze the relationship between the power and frequency of the random signal, the PSD analysis is carried out. The PSD of fixed frequency sinusoidal signal injection scheme and the proposed pseudorandom sinusoidal signal with random winding injection scheme are discussed in this section.

A. Fixed Frequency Sinusoidal Injection

The PSD analysis of the motor current reflects the noise generated in the actual motor operation. In order to present the influence of the injection signal, it is practicable to calculate the PSD of the injection signal and the corresponding response current signal. For the high-frequency sinusoidal voltage injection with fixed frequency scheme, the response current can be expressed as

$$i_h(t) = K_i \int u_{inj} \mathrm{d}t = -\frac{K_i V_h}{\omega_h} \cos(\omega_h t) \tag{23}$$

The PSD of the response current can be expressed as

$$S_F(f) = \left(\frac{K_i V_h}{2\omega_h} \right)^2 \left[\delta(f - f_h) + \delta(f + f_h) \right] \tag{24}$$

where $\delta(f)$ is the unit impulse function, K_i is a coefficient, and f_h is the frequency of the injection signal. Thus, the PSD result produces a high peak at the frequency of the injection signal f_h. It can be concluded that the noise value increases with the increase of the amplitude-frequency ratio of the injected signal.

B. Proposed Pseudorandom Sinusoidal Injection

The PSD of stationary random signals consists of the discrete and continuous spectrum. The noise reduction can be achieved by eliminating the discrete spectrum of the response signal. The random frequency signal can be expressed as

$$i_h^r(t) = \sum_{k=1}^{\infty} i_{h0}^r (t - t_k) \tag{25}$$

When $E[e^{j2\pi fT}] = 1$, the PSD of the random frequency signal can be expressed as

$$S(f) = \frac{1}{\{E[T]\}^2} \left\{ E[|I(f)|] \right\}^2 \tag{26}$$

where $E[]$ represents the mathematical expectation operator, $I(f)$ is the Fourier transform of one cycle of the random frequency signal, T is the period of the random frequency signal. Thus, the discrete spectrum can be eliminated by the following condition as

$$E[|I(f)|] = 0 \tag{27}$$

According to the previous analysis, the proposed pseudorandom sinusoidal signal with random winding injection method consists of three signals. Define the higher frequency voltage signal, lower frequency voltage signals, and null signal as signal 1, signal 2, and signal 3. The frequencies of three signals are f_1, f_2, and null; their periods are T_1, T_2, and T_3 (T_1 or T_2), and probabilities are P_1, P_2, and P_3, respectively. The $E[e^{j2\pi fT}]$ can be calculated as

$$E\left[e^{j2\pi f_v T} \right] = \begin{bmatrix} P_1 & P_2 & P_3 \end{bmatrix} \bullet \left[e^{j2\pi f_v T_1} \quad e^{j2\pi f_v T_2} \quad e^{j2\pi f_v T_3} \right]^T = 1 \tag{28}$$

where $P_1 + P_2 + P_3 = 1$ with $P_1 = 0.25$, $P_2 = 0.25$, and $P_3 = 0.5$.

Assumed that the PSD peaks appear at the frequency f_v. Since signal 3 is null, (28) can be equivalent to

$$e^{j2\pi f_v T_1} = e^{j2\pi f_v T_2} = 1 \tag{29}$$

where the $f_v T_1$ and $f_v T_2$ should be integers. Assumed that the simplest integer ratio of f_1 and f_2 is $f_1/f_2 = k_1 / k_2$, and then the common multiple of f_1 and f_2 is $f_m = k_2 f_1 = k_1 f_2$, yielding

$$f_v = k f_m \tag{30}$$

where k are positive integers. According to the Fourier transform, the following can be obtained as

$$\begin{cases} I_1(f) = \dfrac{jK_i K_v f}{2\pi} \dfrac{1 - e^{-j2\pi f / f_1}}{f^2 - f_1^2} \\ I_2(f) = \dfrac{jK_i K_v f}{2\pi} \dfrac{1 - e^{-j2\pi f / f_2}}{f^2 - f_2^2} \\ I_3(f) = 0 \end{cases} \tag{31}$$

Meanwhile, the component of the discrete spectral peak can be eliminated by

$$I_1(f_v) = I_2(f_v) = I_3(f_v) = 0 \tag{32}$$

When $k_1 > k_2$ and $k_2 > 1$, (32) is completely valid. Thus, there is no discrete spectrum in the PSD of the current signal, which can effectively reduce the acoustic noise caused by the response current. Meanwhile, the injected-frequency component in the winding can be reduced due to the change in mathematical expectation.

V. Experimental Verification

The block diagram of the proposed sensorless control for the DTP-PMSM is shown in Fig. 8. In order to verify the correctness and effectiveness of pseudorandom voltage signal injection method for sensorless control, a surface-mounted DTP-PMSM control platform is established, as shown in Fig. 9. The rated speed, rated torque, and rated current of the DTP-PMSM are 200 r/min, 320 N·m, and 11 A, respectively. The control algorithm is implemented through TMS320F28377. A magnetic powder brake is mechanically coupled with the DTP-PMSM as the load. The mechanical speed and rotor position are measured by using a reluctance resolver. It should be noted that the real speed and position obtained from the encoder are only used for comparison. The sampling frequency and pulse width modulation switching frequency are set to 10 kHz, and the dc-bus voltage is 400 V. The bandwidth of the low-pass filter for the high-frequency signal processing is set as 500 Hz. In order to guarantee the signal-to-noise ratio, the ratio of voltage and frequency of the injection signal is set at 120 V/kHz.

A. PSD results of Phase Currents

The basic injected signal is 48 V 0.4 kHz and 72 V 0.6 kHz. The probability of the higher frequency signal and winding chosen are both 50%. The following experiments are carried out under these conditions. The experimental results for the injected signal and demodulation processing are shown in Fig. 10. The motor is running at 50 r/min with no load. Fig. 10(a) shows the high-frequency currents $i_{\alpha 1h}$, $i_{\alpha 2h}$, and $i_{\alpha h}$. Fig. 10(b) presents the high-frequency currents $i_{\beta 1h}$, $i_{\beta 2h}$, and $i_{\beta h}$. The high-frequency currents in the dq^v-axis are shown in Fig. 10(c). It can be seen that the high-frequency currents in the $\alpha\beta^v$-axis are the position-dependent sine and cosine waves, as shown in Fig. 10(d). Thus, it can be verified that the proposed signal injection method is effective.

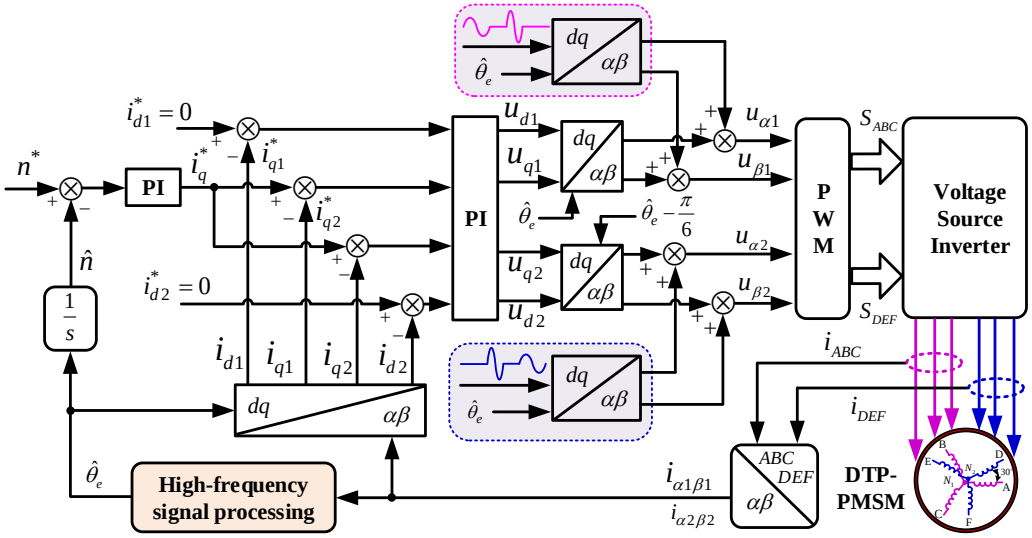

Fig. 8. Block diagram of proposed sensorless control for DTP-PMSM.

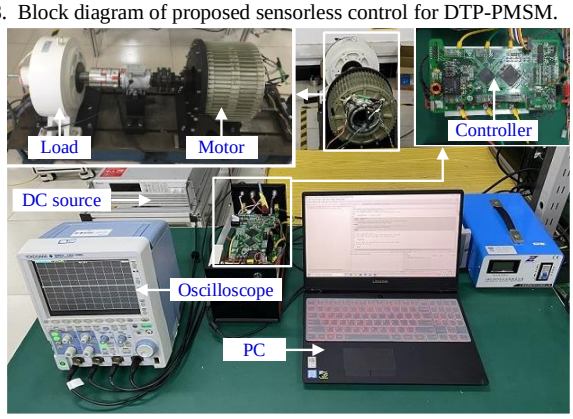

Fig. 9. Experimental platform.

Fig. 11 shows the PSD results of current (phase A) at 50 r/min with rated load. In order to highlight the impact of high-frequency injection signals on the system, Fig. 11(a) presents the PSD result without an injection signal. It can be noticed that there is no obvious peak in the waveform. Figs. 11(b) and 11(c) show the PSD results about fixed frequency injected signal with 48V 0.4 kHz and 72V 0.6 kHz, respectively. The obvious power spectrum peak appears near the frequency of the injected signal. As shown in Fig. 11(b), the maximum amplitude is -4.8 dB, which is located at the frequency of 0.408 kHz. Similarly, the power spectrum peaks appear at 0.589 kHz with an amplitude of -4.23 dB, as shown in Fig. 11(c). The conventional pseudorandom signal injection method performs better in acoustic noise reduction, as shown in Fig. 11(d). Selecting 48 V 0.4 kHz and 72 V 0.6 kHz as the basic high-frequency signals, the probability of high-frequency signal is 50%. It can be seen that the power spectrum peaks at 0.4 kHz and 0.6 kHz are significantly reduced.

In the proposed method, the probabilities of the high-frequency signal and winding chosen are 50%. Fig. 12 shows the PSD results of current (phase A and phase D) at 50 r/min with rated load. The basic injected signal is 48 V 0.4 kHz and 72 V 0.6 kHz. The power spectrum peak appears at 0.418 kHz with an amplitude of -19.9 dB, as shown in Fig. 12(a). Compared with the conventional pseudorandom signal injection method, the power spectrum peak of the proposed method is reduced by 5 dB. It can be concluded that the acoustic noises could be suppressed by the proposed pseudorandom sinusoidal voltage injection with the random winding method.

B. Performance of Sensorless Control

Fig. 13 shows the experimental results under a steady state at 50 r/min with rated load. The currents of phase A and phase D are shown in Fig. 13(a). The maximum amplitude of phase current maintains in the rated value of 11 A. As shown in Fig. 13(b), the real speed and estimated speed maintain at 50 r/min with stable speed error fluctuation. In Fig. 13(c), the estimated position and the real position overlap well. It can be observed that the position error is less than 0.2 rad.

Figs. 14 and 15 show the experimental results of the dynamic performance. In the speed change condition, the motor operates from 50 to -50 r/min under no load condition, as shown in Fig. 14. In Fig. 14(a), the estimated speed traces well with the real speed. The speed error only fluctuates briefly during speed switching. It can be seen that the estimated position match well with the real position. The maximum position estimation error is within 0.35 rad during the speed change.

Fig. 15 shows the experimental results on torque change conditions. The motor operates at 50 r/min, and the magnitude of load torque can be reflected by the amplitude of phase current. In Fig. 15(a), the load torque changes from no load condition to half load condition, then to the no load condition. It can be seen that the real speed decreases while the amplitude increases. The speed error fluctuates a little with a relatively stable value. The maximum fluctuation of position error is about 0.2 rad. Fig. 15(b) presents the performance of position estimation and speed estimation with the torque changes from rated condition to half rated condition. The maximum value of speed error is 6 r/min, which means that the estimated speed matches well with the real speed. Due to the change in motor speed, the position error fluctuates, but it is still less than 0.4 rad. In summary, the proposed pseudorandom sinusoidal voltage with random winding injection method for the DTP-PMSM sensorless drive has a good performance during the steady state and the dynamic process.

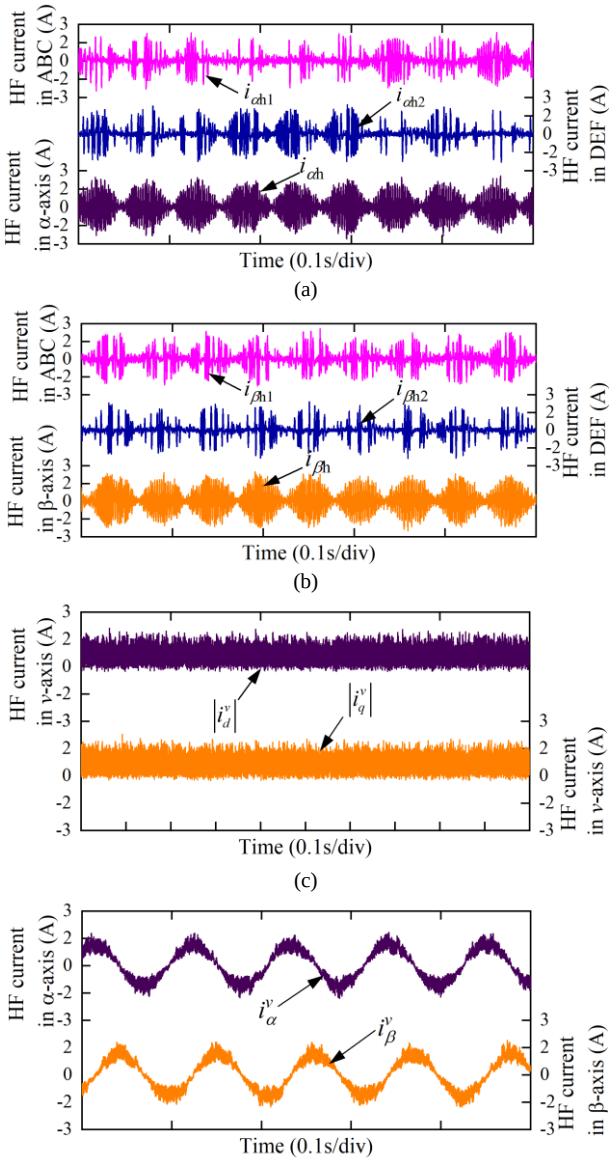

Fig. 10. Experimental results for the injected signal and demodulation processing. (a) High-frequency in α_h-axis. (b) High-frequency in β_h-axis. (c) High-frequency in dq^v-axis. (d) High-frequency in $\alpha\beta^v$-axis.

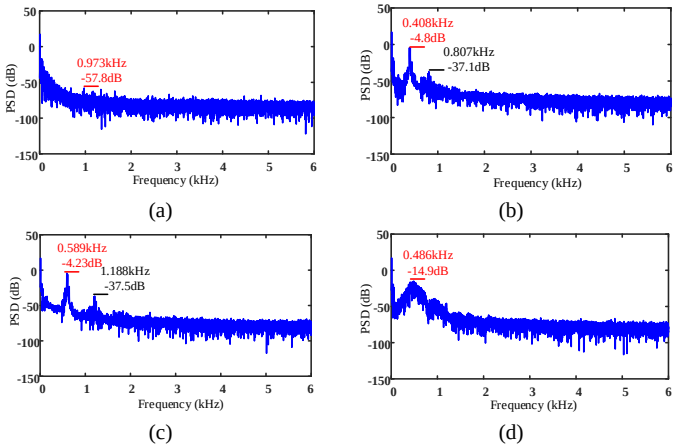

Fig. 11. PSD results of current (phase A). (a) No injection. (b) Fix-frequency 0.4 kHz. (c) Fix-frequency 0.6 kHz. (d) Conventional pseudorandom signal injection method.

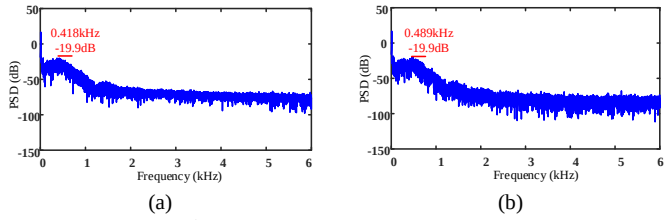

Fig. 12. PSD results of proposed method. (a) Phase A. (b) Phase D.

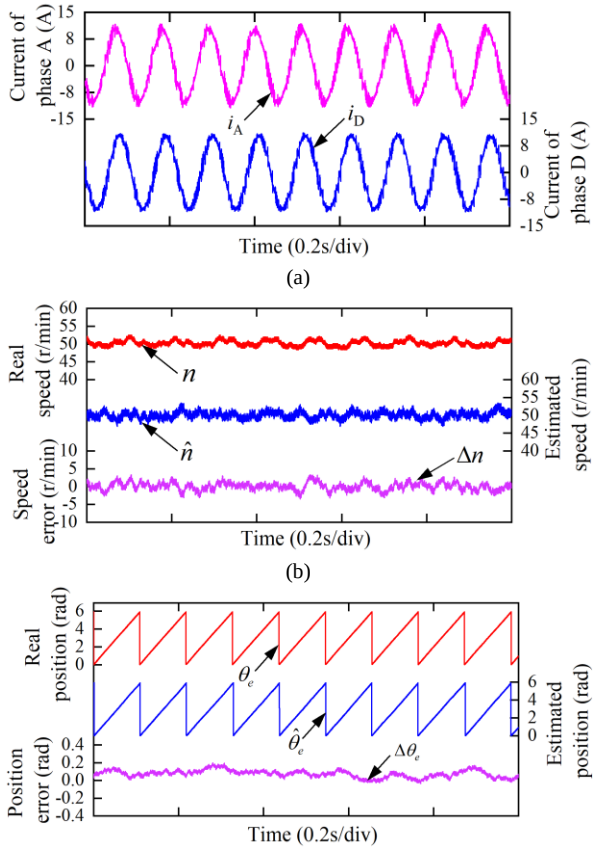

Fig. 13. Position estimation results under a steady-state condition. (a) Currents of phase A and phase D. (b) Speed estimation performance. (b) Position estimation performance.

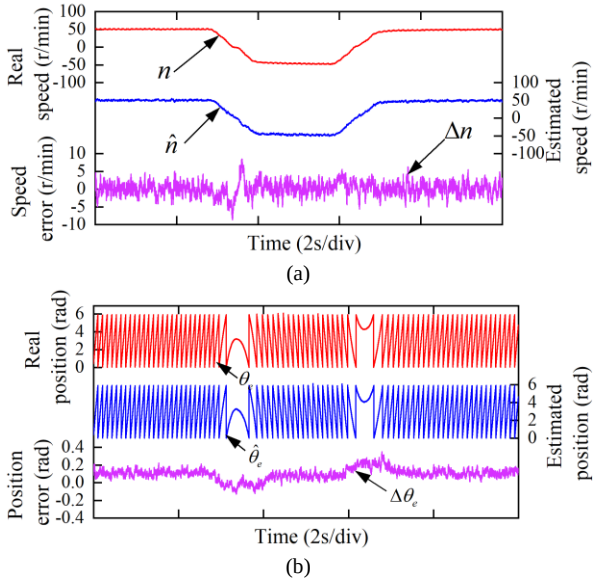

Fig. 14. Experimental results on speed change condition. (a) Speed estimation performance. (b) Position estimation performance.

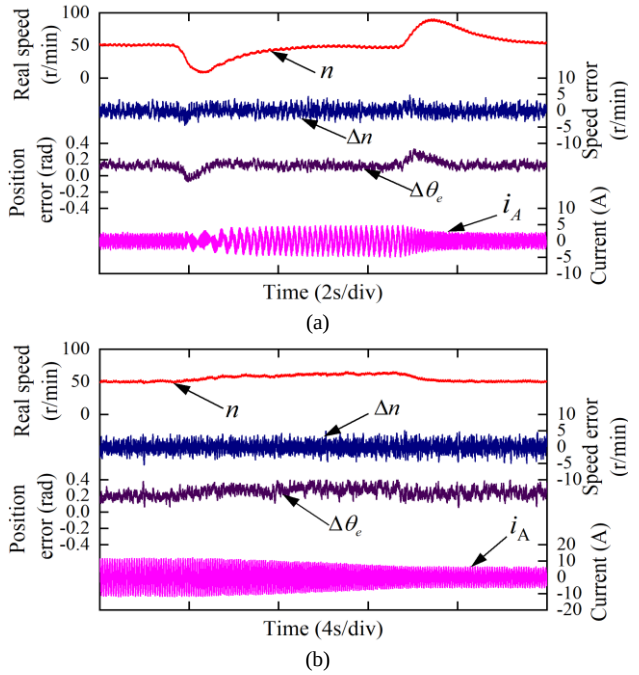

Fig. 15. Experimental results on torque change condition. (a) No load to half rated load, then to no load condition. (b) Rated load to half load condition.

VI. Conclusion

This paper has proposed a pseudorandom sinusoidal signal with random winding injection method for the DTP-PMSM sensorless drive. In order to reduce the acoustic noise caused by the injected signal, pseudorandom sinusoidal voltage is generated and randomly injected into the two sets of windings. The corresponding high-frequency signal processing is designed to demodulate the high-frequency response current. Without the participation of demodulation signal, the position and speed of the DTP-PMSM can be obtained by a phase-lock loop observer. The PSD of response current caused by the injected signal was analyzed. The theoretical analysis shows that the proposed injection method could spread the power spectrum for the injected signal compared to the conventional fixed-frequency sinusoidal voltage injection method. Finally, the correctness and the effectiveness of the proposed method were verified via experiment on a DTP-PMSM drive platform. The experimental results proved that the audible noise could be significantly reduced while ensuring the performance of sensorless drives for the DTP-PMSM.

References

[1] S. V. Nair, K. Layek, and K. Hatua, "An unequal split dual three-phase PMSM with extended torque-speed characteristics for automotive application," *IEEE Trans. Power Electron.,* vol. 37, no. 10, pp. 12437-12449, Oct. 2022.

[2] K. Yu and Z. Wang, "An online compensation method of VSI nonlinearity for dual three-phase PMSM drives using current injection," *IEEE Trans. Power Electron.*, vol. 37, no. 4, pp. 3769-3774, Apr. 2022.

[3] S. Zhu, W. Zhao, G. Liu, Y. Mao, and Y. Sun, "Effect of phase shift angle on radial force and vibration behavior in dual three-phase PMSM," *IEEE Trans. Ind. Electron.*, vol. 68, no. 4, pp. 2988-2998, Apr. 2021.

[4] W. Wang, C. Liu, Z. Song, and Z. Dong, "Harmonic current suppression for dual three-phase PMSM based on deadbeat control and disturbance observer," *IEEE Trans. Ind. Electron.,* doi: 10.1109/TIE.2022.3177818.

[5] B. Zheng, J. Zou, Y. Xu, X. Lang, and G. Yu, "Torque Ripple Suppression Based on Optimal Harmonic Current Injection in Dual Three-Phase PMSMs Under Magnetic Saturation," *IEEE Trans. Ind. Electron.*, vol. 69, no. 6, pp. 5398-5408, Jun. 2022.

[6] L. Huang, J. Ji, T. Tao, Y. Du, and W. Zhao, "Remedial direct torque control for dual three-phase permanent-magnet motor with harmonic torque suppression," *IEEE Trans. Power Electron.*, vol. 37, no. 9, pp. 11085-11097, Sep. 2022.

[7] Z. Novak and M. Novak, "Adaptive PLL-based sensorless control for improved dynamics of high-speed PMSM," *IEEE Trans. Power Electron.*, vol. 37, no. 9, pp. 10154-10165, Sep. 2022.

[8] A. Woldegiorgis, X. Ge, H. Wang, and Y. Zuo, "An active flux estimation in the estimated reference frame for sensorless control of IPMSM," *IEEE Trans. Power Electron.*, vol. 37, no. 8, pp. 9047-9060, Aug. 2022.

[9] D. Wen, W. Wang, and Y. Zhang, "Sensorless control of permanent magnet synchronous motor in full speed range," *Chin. J. Electr. Eng*., vol. 8, no. 2, pp. 97-107, Jun. 2022.

[10] L. Ortombina, M. Berto, and L. Alberti, "Sensorless drive for salient synchronous motors based on direct fitting of elliptical-shape high-frequency currents," *IEEE Trans. Ind. Electron.,* doi: 10.1109/TIE.2022.3177753.

[11] X. Sun, F. Cai, Z. Yang, and X. Tian, "Finite position control of interior permanent magnet synchronous motors at low speed," *IEEE Trans. Power Electron.,* vol. 37, no. 7, pp. 7729-7738, Jul. 2022.

[12] Y. Lee, Y. Kwon, and S. Sul, "Realization of signal-injection sensorless control of SMPMSM with saturation-induced saliency by modification of current trajectory," *IEEE Trans. Power Electron.*, doi: 10.1109/TPEL.2022.3186609.

[13] A. Varatharajan, G. Pellegrino, and E. Armando, "Signal-injection sensorless control of synchronous reluctance machines for overload operation," *IEEE Trans. Power Electron.*, vol. 37, no. 5, pp. 5874-5883, May 2022.

[14] J. Sun, J. Zhao, L. Tian, Y. Song, and Y. Liu, "Bandwidth and audible noise improvement of sensorless IPMSM drives based on amplitude modulation multi-random frequency injection," *IEEE Trans. Power Electron.*, doi: 10.1109/TPEL.2022.3187535.

[15] W. Qian, X. Zhang, F. Jin, H. Bai, and D. Lu, "Using high-control bandwidth FPGA and SiC inverters to enhance high-frequency injection sensorless control in interior permanent magnet synchronous machine," *IEEE Access*, vol. 6, pp. 42454-42466, Jul. 2018.

[16] G. Wang, D. Xiao, N. Zhao, X. Zhang, W. Wang, and D. Xu, "Low-frequency pulse voltage injection scheme-based sensorless control of IPMSM drives for audible noise reduction," *IEEE Trans. Ind. Electron.*, vol. 64, no. 11, pp. 8415-8426, Nov. 2017.

[17] G. Wang, L. Yang, G. Zhang, X. Zhang, and D. Xu, "Comparative investigation of pseudorandom high-frequency signal injection schemes for sensorless IPMSM drives," *IEEE Trans. Power Electron.*, vol. 32, no. 3, pp. 2123-2132, Mar. 2017.

[18] G. Zhang, R. Xiang, G. Wang, et al., "Hybrid pseudorandom signal injection for position sensorless SynRM drives with acoustic noise reduction," *IEEE Trans. Transport. Electrific.*, vol. 8, no. 1, pp. 1313-1325, Mar. 2022.

[19] G. Zhang, G. Wang, H. Wang, D. Xiao, L. Li, and D. Xu, "Pseudorandom-frequency sinusoidal injection based sensorless IPMSM drives with tolerance for system delays," *IEEE Trans. Power Electron.*, vol. 34, no. 4, pp. 3623-3632, Apr. 2019.

[20] J. Chen, Y. Fan, W. Wang, C. H. Lee, and X. Wang, "Sensorless control for synRM drives using a pseudo-random high-frequency triangular-wave current signal injection scheme," *IEEE Trans. Power Electron.*, vol. 37, no. 6, pp. 7122-7131, Jun. 2022.

[21] B. Du, T. Zhao, S. Han, L. Song, and S. Cui, "Sensorless control strategy for IPMSM to reduce audible noise by variable frequency current injection," *IEEE Trans. Ind. Electron.*, vol. 67, no. 2, pp. 1149-1159, Feb. 2020.

[22] Z. Yang, K. Wang, and X. Sun, "Novel random square-wave voltage injection method based on markov chain for IPMSM sensorless control," *IEEE Trans. Power Electron.*, doi: 10.1109/TPEL.2022.3181173.

[23] Y. Zhang, Z. Yin, C. Du, J. Liu, and X. Sun, "Noise spectrum shaping of random high-frequency-voltage injection based on markov chain for IPMSM sensorless control," *IEEE Trans. J. Emerg. Sel. Topics Power Electron.*, vol. 8, no. 4, pp. 3682-3699, Dec. 2020.

[24] Y. Zhang, Z. Yin, J. Liu, R. Zhang, and X. Sun, "IPMSM sensorless control using high-frequency voltage injection method with random switching frequency for audible noise improvement," *IEEE Trans. Ind. Electron.*, vol. 67, no. 7, pp. 6019-6030, Jul. 2020.